ACCSCIENCE PUBLISHING

International Journal of AI for Materials and Design

ORIGINAL RESEARCH ARTICLE

Data-driven optimization of biaxial shrinkage and stability in electrospun membranes via machine learning and Monte Carlo simulation

Shiyu He[1,2], Chentong Gao[2,3], Runzhi Lu[2,4], Fei Xiao[1,5]*, Li Cong Huang[6], and Wei Min Huang[2]*

[1]State Key Laboratory of Metal Matrix Composites, School of Materials Science and Engineering, Shanghai Jiao Tong University, Shanghai, China

[2]School of Mechanical and Aerospace Engineering, Nanyang Technological University, Singapore

[3]College of Aerospace Engineering, Nanjing University of Aeronautics and Astronautics, Nanjing, Jiangsu, China

[4]School of Civil Engineering, Southeast University, Nanjing, Jiangsu, China

[5]Department of Computer Science, Institute of Medical Robotics, Shanghai Jiao Tong University, Shanghai, China

[6]School of Computing, National University of Singapore, Singapore

***Corresponding authors:**
Fei Xiao
(xfei@sjtu.edu.cn)
Wei Min Huang
(mwmhuang@ntu.edu.sg)

Citation: He S, Gao C, Lu R, Xiao F, Huang LC, Huang WM. Data-driven optimization of biaxial shrinkage and stability in electrospun membranes via machine learning and Monte Carlo simulation. *Int J AI Mater Design*. 2025;2(3):64-77.
doi: 10.36922/IJAMD025260022

Received: June 26, 2025

Revised: August 15, 2025

Accepted: August 21, 2025

Published online: September 9, 2025

Abstract

Controlling shrinkage behavior in electrospun membranes is critical for applications that require precise dimensional or mechanical performance. However, experimental variability and limited datasets often hinder the development of robust process models. This study introduces a data-driven framework that combines machine learning with Monte Carlo simulation to enable both accurate and stable shrinkage control in electrospinning using a small experimental dataset. Multiple regression models were trained to predict biaxial shrinkage ratios and their variability, with support vector regression and extreme gradient boosting showing the best performance for accuracy and stability prediction, respectively. Feature importance analysis revealed applied voltage and thermoplastic polyurethane concentration as the dominant parameters. A Monte Carlo-based optimization strategy was employed to identify process parameter sets that achieve target shrinkage ratios while minimizing output variability. The proposed approach enables multi-objective optimization in low-data, high-variability manufacturing environments, offering practical insights into precision fabrication of stimulus-responsive membranes.

Keywords: Electrospinning; Shrinkage stability; Machine learning; Monte Carlo simulation; Process parameter optimization

1. Introduction

Electrospinning has become a key nanofabrication technique in biomedical and engineering applications due to its simplicity, material adaptability, and ability to produce continuous fibers with diameters ranging from nanometers to micrometers.[1-3] Electrospun membranes, such as polyvinyl alcohol, poly(lactic acid), poly(lactide-co-glycolide), are widely employed in tissue engineering, drug delivery, smart materials, flexible electronics,

and filtration systems.[4-6] Notably, these membranes often undergo spontaneous and stimulus-responsive shrinkage when exposed to thermal, solvent, or moisture-based triggers.[7,8] Such shrinkage enables functional transformations, such as self-folding structures, yet its anisotropy and instability can cause severe deformation, critically limiting its reliability in applications such as tissue scaffolds.[9,10]

Recent studies suggest that the shrinkage of electrospun membranes originates from a gradient prestrain field within the cross-sectional area generated during fiber formation, driven by radial differences in solvent evaporation, prestraining from high-speed collectors, and the rapid fixation of polymer chain orientation.[11,12] Upon exposure to external stimuli, such as solvents, the shape memory effect[13,14] activates the prestrain, causing fiber buckling and resulting in macroscopic, anisotropic membrane contraction. Despite these insights, current models remain largely qualitative. Shrinkage control continues to rely on empirical parameter adjustments, lacking a predictive, quantitative framework capable of capturing the non-linear, multivariable nature of the process and its sensitivity to perturbations.[11]

Subtle variations in electrospinning parameters, such as applied voltage, rotation speed of the collator, distance between electrodes, and solvent concentration, can significantly affect jet dynamics, fiber solidification, and internal prestrain distribution, resulting in anisotropic and often unpredictable shrinkage behavior.[15] Due to the non-linear and multivariable nature of these effects, traditional modeling approaches often lack the accuracy and generalizability required for effective control.[16] Moreover, electrospinning experiments are typically labor-intensive and sensitive to environmental fluctuations, hindering the acquisition of high-throughput data.[17] As a result, available datasets are often limited in size and scope, further constraining the development of robust process control strategies.

Based on the experimental data reported in literature,[11] Figure 1 illustrates the distribution of system outputs along the rotational and transverse axes, with each data cluster (applied voltage [kV], rotation speed of collator [rpm], distance between electrodes [cm], and solvent concentration [%]) corresponding to a distinct combination of input parameters, denoted by unique "Combo" identifiers. To enable quantitative interpretation of cluster behavior, each group of data points is enclosed by a Gaussian confidence ellipse delineating the 68% probability region. These ellipses are computed based on the Mahalanobis distance, which incorporates the full covariance structure of each cluster to account for correlations and anisotropic variance. In contrast to Euclidean distance, the Mahalanobis metric provides scale-invariant and directionally sensitive distance measures, thereby yielding ellipses that more accurately reflect the underlying multivariate normal distribution of the data. The adoption of a 68% confidence level corresponds to one standard deviation from the mean in the bivariate normal case, thereby capturing the most statistically representative core of each distribution, while reducing sensitivity to outliers and extreme observations. This visualization framework supports inverse mapping, i.e., given a desired target output, its location on the plot can be used to identify the nearest confidence ellipse, and thus infer the most probable input parameter configuration that can produce the specified response. This approach enables principled, data-informed decision-making in predictive modeling and design selection.

According to Figure 1, the experimentally obtained biaxial shrinkage ratios only cover certain discrete regions. The same region can be covered by different combinations of processing parameters. Even when using identical parameters, the degree of result dispersion varies significantly depending on the parameter combination used. How can we optimally select a combination of processing parameters to achieve the desired biaxial shrinkage ratios of the electrospun membrane while minimizing variability?

More broadly, optimizing processing parameters in manufacturing is essential not only for achieving target performance but also for ensuring product stability and consistency across production. In processes such as electrospinning, small variations in parameters can lead to significant fluctuations in fiber morphology, internal stress distribution, and functional outcomes. With the recent emergence of machine learning in membrane science, there is increasing potential to address these challenges by enabling data-driven process optimization that simultaneously targets performance and stability, as demonstrated in recent studies on material discovery, process control, and performance prediction.[18-20] However, many artificial intelligence (AI)-based approaches focus primarily on predicting average performance, often overlooking process variability and robustness.[21] This limitation is particularly evident under small-sample conditions, where models may capture central trends but fail to reflect sensitivity to parameter fluctuations.[22] As a result, predictions may meet nominal targets while real-world performance remains unstable. Integrating both accuracy and stability into modeling frameworks is therefore vital for reliable, data-driven optimization in high-variability manufacturing scenarios.

More broadly, optimizing processing parameters in manufacturing is crucial not only to meet performance standards but also to ensure consistent product stability.

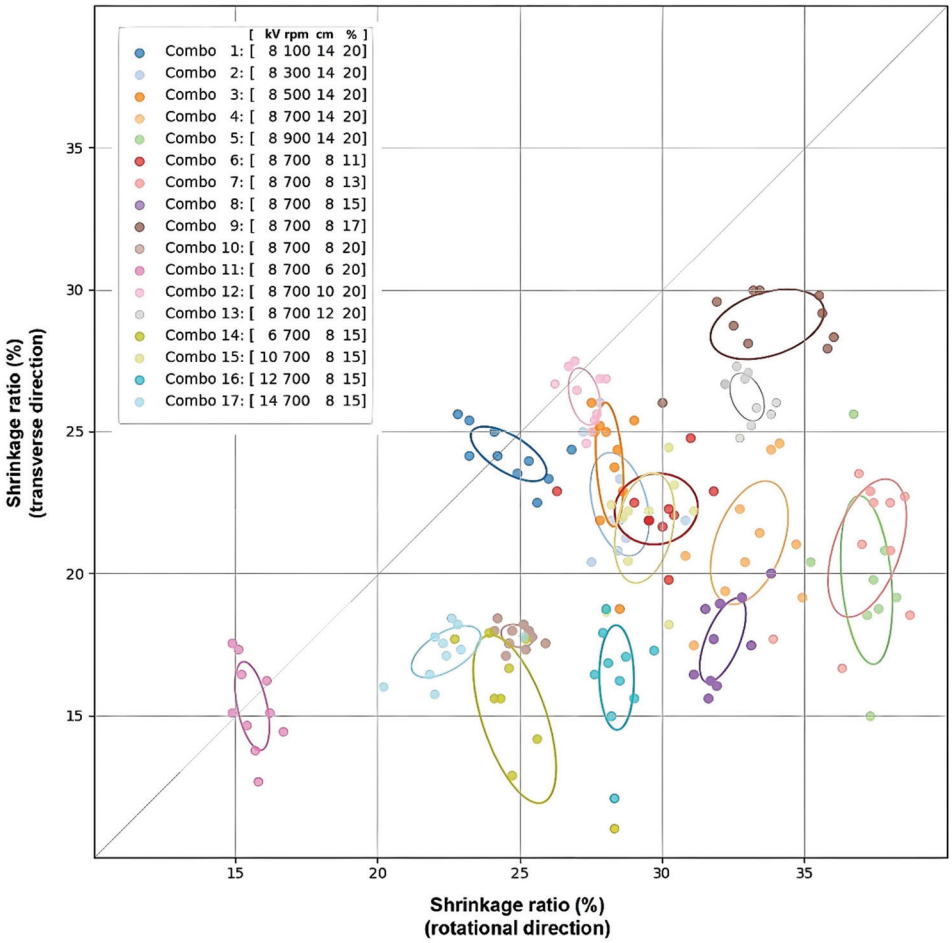

Figure 1. Scattered plot of measured shrinkage ratios in the transverse direction and rotational direction of each membrane in the literature,[11] with clusters highlighted and inner confidence contours

However, current AI applications largely focus on achieving performance targets, often neglecting stability, especially when data are limited.

To address these challenges, this study proposes a hybrid approach that integrates machine learning with Monte Carlo simulation to model and analyze the shrinkage behavior and stability of electrospun membranes based on a limited experimental dataset. A supervised learning model is first developed using experimental data (from literature;[11] Figure 1) to capture the non-linear relationships between processing parameters and shrinkage ratios under multifactorial conditions. On the other hand, a shrinkage stability coefficient is introduced to quantify the sensitivity of shrinkage to parameter perturbations, and the Monte Carlo simulation is employed to characterize its statistical distribution. This framework enables the identification of a controllable processing parameter space that ensures both target biaxial shrinkage performance and robustness in biaxial shrinkage. The proposed methodology establishes a data-driven and uncertainty-aware paradigm, offering both theoretical and practical guidance for designing tunable and stimulus-responsive electrospun membranes.

2. Methodology

This study presents a data-driven framework for optimizing electrospinning processes, which focuses on shrinkage behavior and stability. The proposed methodology consists of three main components: (i) dataset construction based on experimental measurements under controlled parameter variations; (ii) development and interpretation of machine learning models for predicting shrinkage ratios and their stability; and (iii) a Monte Carlo simulation-based strategy for identifying process conditions that satisfy target shrinkage values, while ensuring minimal variability.

2.1. Dataset construction

To develop a predictive and robust model for shrinkage behavior in electrospun membranes, we constructed an

experimental database from controlled electrospinning tests using thermoplastic polyurethane (TPU) solutions. Shrinkage ratios in the rotational direction (RD) and transverse direction (TD) were obtained by measuring the linear dimensions of the membrane before and after ethanol activation, where RD is parallel to the axis of rotation of the roller collector and TD is perpendicular to it. The shrinkage ratio in each direction was calculated as the percentage reduction in length relative to the initial length, that is, the difference between the initial and final lengths divided by the initial length. The four input features (solvent concentration, distance between electrodes, collector speed, and applied voltage) were selected for their direct influence on jet formation, fiber deposition, and solvent evaporation, which together determine the internal prestrain distribution. The solution flow rate was maintained at a fixed constant value throughout all experiments to avoid introducing additional variability from unstable jet formation. Each parameter combination was tested at least five times under controlled conditions, revealing up to 10% variation in shrinkage ratios under identical settings. This variability was expressed as the confidence interval width (CIW), the range between the upper and lower bounds of the 95% confidence interval, with a smaller CIW indicating higher stability. CIW was used as the stability metric alongside mean shrinkage values. The dataset spans practical parameter ranges, ensuring representativeness and reliability for model training. The details of the materials and experimental procedures are described in.[11] The measured shrinkage ratios (%RD and %TD) of each tested membrane are presented in Figure 1.

2.2. Model development and interpretation

In this study, predictive models were developed for both the shrinkage ratio and shrinkage stability. The shrinkage stability metric was defined based on the CIW of repeated measurements under identical processing conditions, with lower values indicating higher process robustness and consistency. To identify the most effective predictive model for shrinkage behavior, several machine learning algorithms were assessed, including support vector regression (SVR),[23] random forest (RF),[24] extreme gradient boosting (XGBT),[25] artificial neural networks (ANN),[26] and linear regression (LR).[27] These models were selected to cover kernel-based, ensemble, neural network, and linear paradigms, offering complementary strengths for small-sample, non-linear, and high-variability systems, and providing a balanced basis for robust model selection.

The dataset was randomly partitioned into a training set (80%) and a testing set (20%) to ensure robust model validation. Each model was trained to establish the non-linear mapping from processing parameters (applied voltage, TPU concentration, collector speed, electrode distance) to shrinkage ratios (%RD and %TD). Model performance was evaluated on the testing set using a set of complementary metrics, including mean squared error (MSE), root mean square error (RMSE), mean absolute error (MAE), mean absolute percentage error (MAPE), coefficient of determination (R^2), and Pearson correlation coefficient (R). These metrics capture different aspects of predictive accuracy: MSE and RMSE emphasize penalization of large errors, MAE reflects the average magnitude of deviation, MAPE provides a relative error assessment normalized to the scale of measurement, and R^2, along with R, quantify the proportion of variance explained and the degree of linear correlation between predicted and observed values. The optimal model was selected based on a composite assessment of these metrics. Priority was given to models achieving low error values (MSE, RMSE, and MAE) and high consistency indicators (R^2, R). The selected model was then integrated into the stability evaluation framework, providing a reliable predictive core for Monte Carlo-based optimization.

Subsequently, the Shapley Additive Explanations (SHAP) method[18,28-33] was applied to interpret the trained model and reveal the relationship between electrospinning parameters and shrinkage behavior. This analysis enabled the identification of key process features that most strongly influence shrinkage, providing a clear basis for understanding and optimizing critical factors in membrane fabrication. Mathematically, SHAP values are derived from the cooperative game theory framework, where each feature is considered a "player" contributing to the model prediction. For a model prediction $f(x)$, the SHAP value for the i^{th} feature is computed with Equation I,

$$\phi_i = \sum_{S \subseteq N \setminus \{i\}} \frac{|S|!\left(M-|S|-1\right)!}{M!}\left[f_{S\cup\{i\}}\left(x_{S\cup\{i\}}\right) - f_S\left(x_S\right)\right] \quad \text{(I)}$$

where M is the total number of features, S represents a subset of features excluding i; $f_S(x_S)$ is the model output when only features in S are included; ϕ_i quantifies the average marginal contribution of feature i over all possible feature combinations.

In the context of this study, the trained regression model $f(x)$ maps the four process parameters (voltage, TPU concentration, collector speed, and electrode distance) to the predicted shrinkage ratios and stability. The SHAP value ϕ_i for each parameter represents its average contribution to increasing or decreasing the predicted shrinkage outcome, aggregated over all permutations of feature inclusion. By summing all contributions and the

base value f_0 (mean model output), the prediction can be decomposed as Equation II.

$$f(x) = f_0 + \sum_{i=1}^{M} \phi_i \quad \text{(II)}$$

This additive decomposition provides a transparent interpretation of how each electrospinning parameter affects the model output, enabling a parameter-sensitive optimization strategy.

2.3. Optimization of shrinkage stability

To identify optimal processing parameters that achieve target shrinkage ratios with maximal stability, a Monte Carlo simulation[34-38] framework was established by integrating shrinkage prediction and shrinkage stability models. The Monte Carlo method is a stochastic simulation technique that estimates numerical results by performing repeated random sampling over the parameter space. In this study, each process parameter, including applied voltage, TPU concentration, collector speed, and electrode distance, is treated as a random variable within experimentally feasible bounds. A large number N of parameter sets is generated from the joint distribution of process parameters to explore the multidimensional process space in an unbiased and comprehensive manner. Compared with Bayesian optimization or other sequential search algorithms, this one-step large-scale sampling can simultaneously evaluate shrinkage accuracy and stability without iterative model updates, making it particularly suitable for our non-linear, high-variability system with a pre-trained predictive model.

Mathematically, for a target shrinkage function $f(x)$ and stability metric $g(x)$, the expected values are approximated as Equation III,

$$E[f(x)] \approx \frac{1}{N}\sum_{k=1}^{N} f(x_k), E[g(x)] \approx \frac{1}{N}\sum_{k=1}^{N} g(x_k) \quad \text{(III)}$$

where x_k is the kth random sample of process parameters. Through sufficient sampling, the distribution of predicted shrinkage ratios (%RD, %TD) and stability coefficient (CIW) can be estimated.

By filtering all samples that meet the target shrinkage tolerance, the Monte Carlo method provides a numerical approximation to the feasible design domain. The subsequent ranking by predicted CIW corresponds to an optimization over the estimated probability distribution of outcomes. This enables the selection of parameter combinations that maximize process robustness while satisfying the desired biaxial shrinkage performance. The method proceeds as follows:

(i) Step 1: Initialization
The optimization process begins by specifying the target shrinkage ratios in the radial direction (RD) and TD, denoted as R_{RD}^{target} and R_{TD}^{target}. In addition, tolerance limits Δ_{RD} and Δ_{TD} are defined to account for permissible deviations from the target values. These targets are determined based on the desired dimensional accuracy of the electrospun mat after post-processing, ensuring the end product meets application-specific requirements (e.g., biomedical scaffolds or filtration membranes). This initialization step provides clear quantitative objectives for subsequent parameter screening.

(ii) Step 2: Monte Carlo sampling
A large set of candidate processing parameter combinations is generated via Monte Carlo sampling within predefined practical ranges. The considered parameters include applied voltage (kV), solution concentration (wt%), collector distance (cm), and rotation speed (rpm). Random sampling ensures comprehensive coverage of the parameter space, enabling the identification of non-intuitive optimal combinations that conventional trial-and-error methods may miss.

(iii) Step 3: Shrinkage prediction
Each sampled parameter set is evaluated using a previously trained shrinkage prediction model, which was constructed based on experimental data and machine learning algorithms. The model outputs predicted shrinkage ratios in $RD\left(\hat{R}_{RD}\right)$ and $TD\left(\hat{R}_{TD}\right)$, capturing the non-linear dependencies between processing parameters and shrinkage behavior. This predictive approach greatly reduces the number of costly experimental trials.

(iv) Step 4: Feasibility filtering
Only those parameter sets whose predicted shrinkage ratios satisfy Equation IV,

$$|\hat{R}_{RD} - R_{RD}^{target}| \leq \Delta_{RD}, |\hat{R}_{TD} - R_{TD}^{target}| \leq \Delta_{TD} \quad \text{(IV)}$$

are retained for further analysis. This filtering step eliminates parameter combinations that would produce excessive dimensional deviation, thus narrowing the candidate pool to only potentially viable solutions.

(v) Step 5: Stability assessment
For each feasible parameter set, shrinkage stability is evaluated using a trained stability prediction model. The stability metric is expressed as the predicted CIW, which reflects the sensitivity of shrinkage behavior to process fluctuations. A smaller CIW corresponds to a more robust process configuration, less prone to variation due to environmental changes or equipment drift. This step ensures that the selected parameters are not only accurate but also reproducible in real production.

(vi) Step 6: Pareto front construction
The feasible samples are mapped onto a Pareto front by jointly considering two competing objectives: Shrinkage deviation from the target values and the predicted CIW (robustness). This multi-objective optimization framework enables the identification of trade-offs between dimensional accuracy and process stability, guiding informed decision-making rather than relying on a single metric.

(vii) Step 7: Optimal parameter selection.
Based on the Pareto front constructed in Step 6, the optimal processing configuration is selected by prioritizing the lowest CIW to maximize stability while maintaining an acceptable deviation from the target shrinkage ratios, ensuring dimensional precision. This integrated approach effectively balances product quality with manufacturing consistency, providing a practical and reliable processing window for electrospinning applications.

3. Results and discussion

3.1. Shrinkage ratio prediction model

Figure 2 illustrates the predictive performance of six machine learning models in estimating the shrinkage ratio in the %RD, namely RF, SVR, XGBT, ANN, decision tree regressor (DTR), and LR. Among them, RF, SVR, and XGBT exhibit high prediction accuracy, as evidenced by the close alignment of predicted values with the ideal diagonal line on both training and test sets, indicating strong generalization capability across varying input conditions. The ANN, DTR, and LR models display noticeably larger deviations from the ground truth, suggesting the presence of underfitting, model bias, or limited capacity to capture the complex, non-linear relationships inherent in the dataset. Notably, certain predicted %RD values correspond to multiple experimentally observed outcomes. This phenomenon does not originate from predictive ambiguity in the models but rather reflects the intrinsic instability of the electrospinning process itself. The shrinkage ratios are susceptible to fluctuations arising from subtle variations in ambient environment, equipment status, and material heterogeneity, all of which can introduce non-negligible noise into the output. Such variability highlights the necessity of incorporating both accuracy and stability into the modeling framework to ensure reliable shrinkage control.

Figure 3 presents the performance of six machine learning models in predicting %TD, including RF, SVR, XGBT, ANN, DTR, and LR. Among them, RF, SVR, and XGBT achieve relatively accurate predictions on both training and test sets, with predicted values closely matching observed values, and the points clustering tightly around

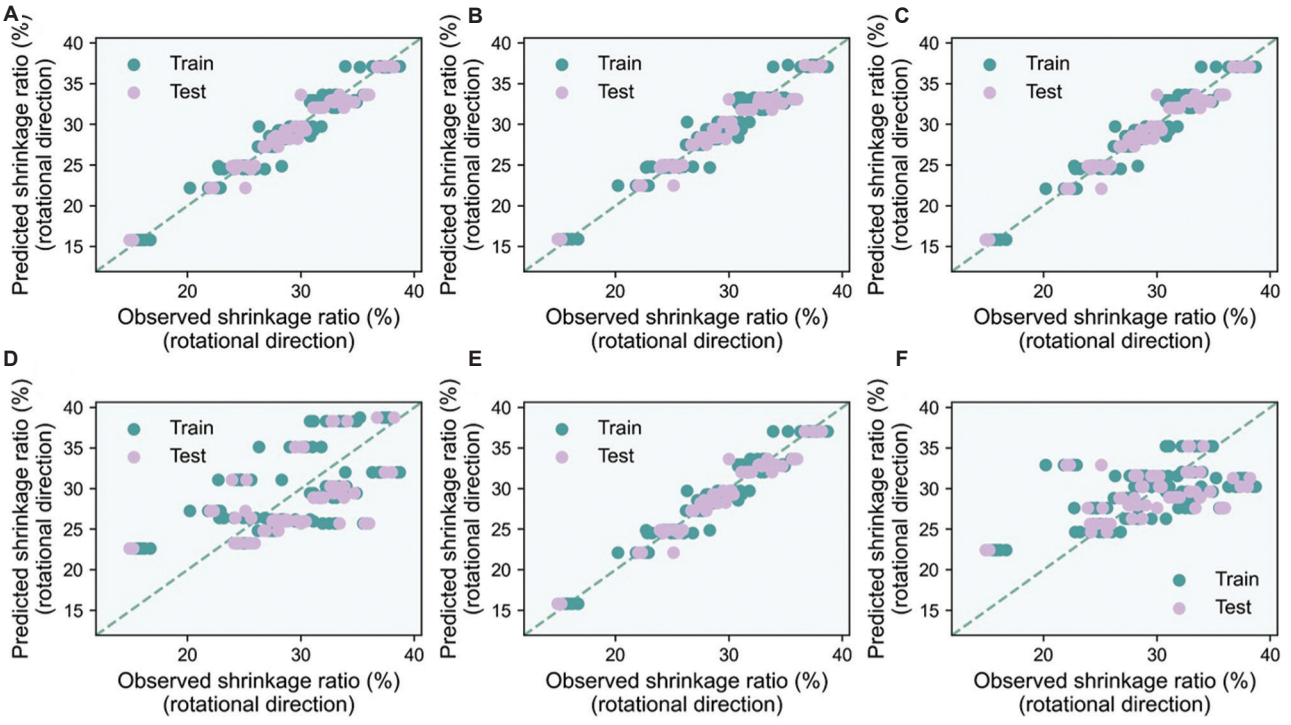

Figure 2. Performance of different machine learning models in predicting the percentage of rotational direction on the test set. (A) Random forest. (B) Support vector regression. (C) Extreme gradient boosting trees. (D) Artificial neural networks. (E) Decision tree regressor; (F) Linear regression.

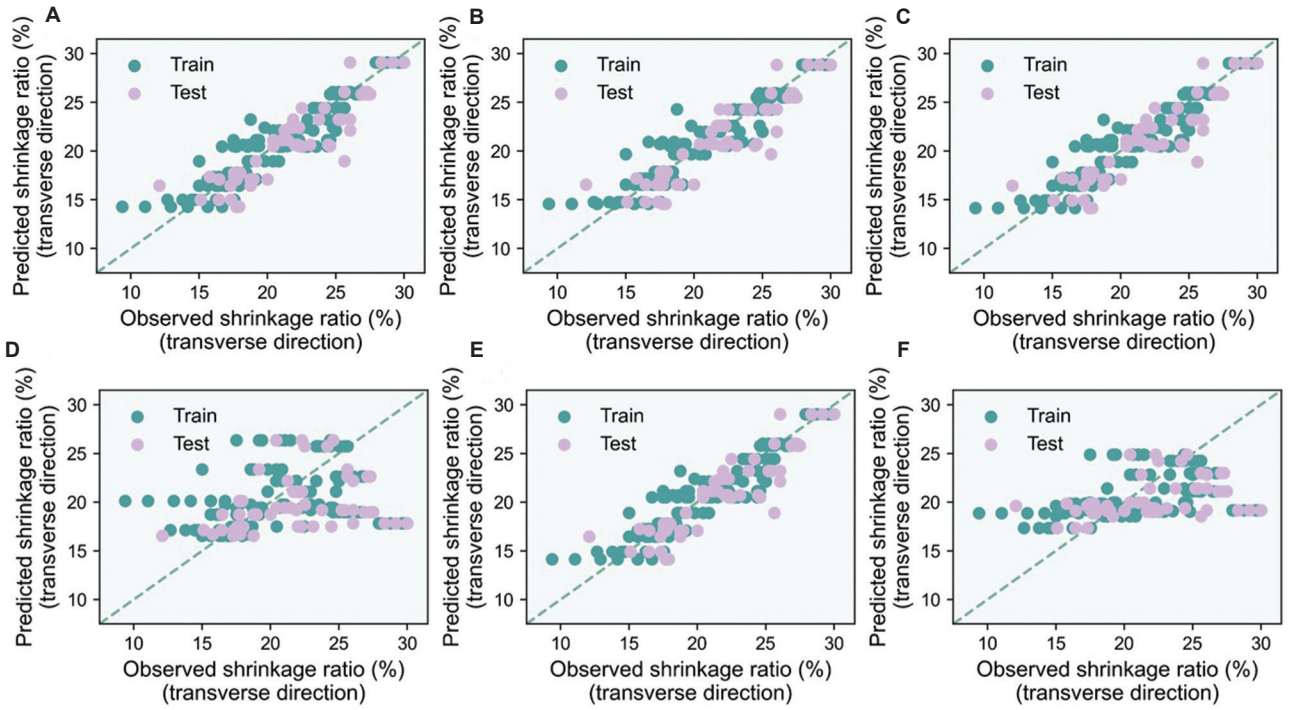

Figure 3. Performance of different machine learning models in predicting the percentage of transverse direction on the test set. (A) Random forest. (B) Support vector regression. (C) Extreme gradient boosting trees. (D) Artificial neural networks. (E) Decision tree regressor; (F) Linear regression.

the diagonal line. The SVR and XGBT models demonstrate slightly better consistency and convergence, particularly on the test set, which suggests that they are more robust in handling high-dimensional interactions under small-sample conditions. However, the ANN and LR models exhibit considerably lower predictive accuracy, particularly on the test set. The ANN model, while theoretically capable of modeling non-linearities, shows significant scatter in the prediction results, indicating that it may have overfit the training data or failed to generalize due to limited data and suboptimal hyperparameter tuning. The LR model, which relies on a strictly linear approximation of the feature space, consistently underperforms across the entire prediction range, suggesting that it is fundamentally inadequate for capturing the multivariate non-linear dependencies inherent in the electrospinning process.

Table 1 presents the performance comparison of different machine learning models in predicting %RD and %TD. The RF, SVR, XGBT, and DTR models exhibit relatively low prediction errors (MSE = 1.04–1.10, MAE = 0.74–0.79, MAPE = 2.6–2.8) and high goodness-of-fit metrics (R^2 = 0.96, R = 0.98). Notably, the SVR, XGBT, and DTR models achieve the highest R^2 (0.96), indicating excellent predictive performance for %RD. In the case of %TD prediction, the SVR model demonstrates superior performance, achieving the lowest MSE (4.00),

Table 1. Performance comparison of different machine learning models in predicting %RD and %TD evaluated by MSE, RMSE, MAE, MAPE, R^2, and R

Properties	Model	MSE	RMSE	MAE	MAPE	R^2	R
%RD	RF	1.1	1.05	0.79	2.78	0.96	0.98
	SVR	1.04	1.02	0.74	2.59	0.96	0.98
	XGBT	1.04	1.02	0.74	2.59	0.96	0.98
	ANN	19.38	4.4	3.82	14.03	0.27	0.59
	DTR	1.04	1.02	0.74	2.59	0.96	0.98
	LR	19.62	4.43	3.32	12.55	0.26	0.52
%TD	RF	4.08	2.02	1.51	7.2	0.74	0.9
	SVR	4	2	1.53	7.35	0.75	0.9
	XGBT	4.13	2.03	1.53	7.27	0.74	0.9
	ANN	19.45	4.41	3.24	13.89	-0.23	0.35
	DTR	4.13	2.03	1.53	7.27	0.74	0.9
	LR	14.74	3.84	2.94	13.16	0.07	0.42

Abbreviations: %RD: Shrinkage ratio (%) in rotational direction; %TD: Shrinkage ratio (%) in transverse direction; ANN: Artificial neural networks; DTR: Decision tree regressor; LR: Linear regression; MAE: Mean absolute error; MAPE: Mean absolute percentage error; MSE: Mean squared error; R: Pearson correlation coefficient; R^2: Coefficient of determination; RF: Random forest; RMSE: Root mean square error; SVR: Support vector regression; XGBT: Extreme gradient boosting trees.

the smallest RMSE (2.00), the highest R^2 (0.75), and a relatively low MAPE (7.35). In contrast, the RF, XGBT, and DTR models exhibit higher prediction errors in %TD forecasting. The ANN and LR models perform poorly across both tasks, with particularly unsatisfactory results from the ANN model in %TD prediction, where it yields a negative R^2 (−0.23), likely due to the limited dataset size and suboptimal model parameterization. The relatively lower accuracy for %TD compared with %RD can be attributed to its higher experimental variability and sensitivity to uncontrolled factors, such as ambient humidity and fiber deposition heterogeneity, which were not included in the model inputs.

3.2. Shrinkage stability prediction model

Figure 4 illustrates the performance of six machine learning models in predicting the stability of %RD, including RF, SVR, XGBT, ANN, DTR, and LR. Figure 4A-F presents the comparison between the predicted and actual observed values on both the training and testing sets for each model, while Figure 4G-I depicts the evaluation metrics MSE, RMSE, and MAE on the testing set. From the scatter plots

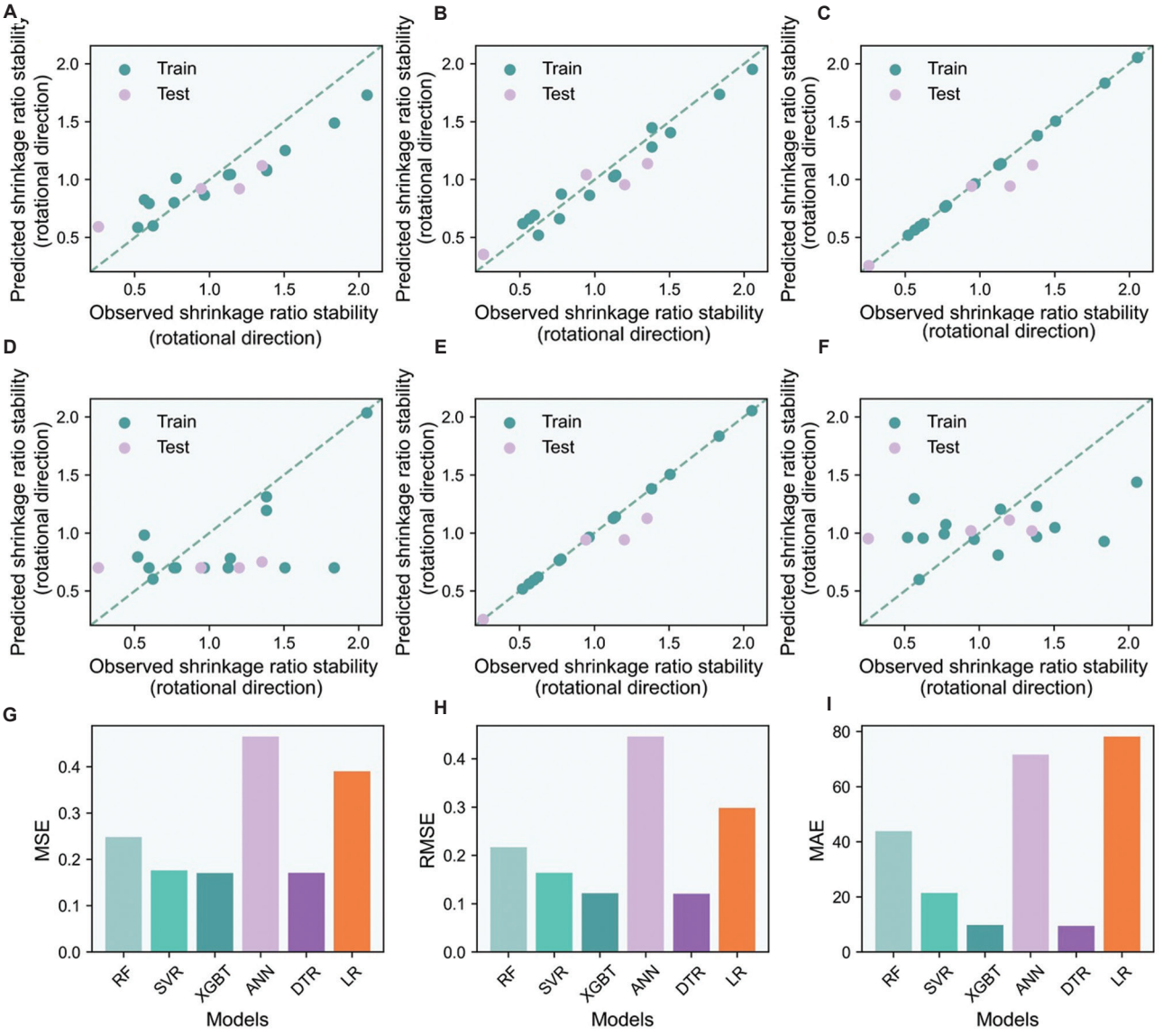

Figure 4. Performance of different machine learning models in predicting the stability of %RD on the test set. (A) RF. (B) SVR. (C) XGBT. (D) ANN. (E) DTR. (F) LR. (G) MSE of the models. (H) RMSE of the models. (I) MAE of the models.

Abbreviations: %RD: Shrinkage ratio (%) in rotational direction; ANN: Artificial neural networks; DTR: Decision tree regressor; LR: Linear regression; MAE: Mean absolute error; MSE: Mean squared error; RF: Random forest; RMSE: Root mean square error; SVR: Support vector regression; XGBT: Extreme gradient boosting trees.

(Figure 4A-F), it is evident that the XGBT and DTR models produce predictions that are more closely aligned with the ideal diagonal line on the test set, indicating superior fitting accuracy and generalization performance. In contrast, the LR, ANN, and SVR models exhibit larger deviations in their predictions. In terms of error metrics, the XGBT and DTR models achieve the lowest values across all three indicators (MSE, RMSE, and MAE), demonstrating the highest accuracy in capturing variations in %RD stability.

Figure 5 presents the performance of six machine learning models in predicting %TD stability, including RF, SVR, XGBT, ANN, DTR, and LR. The fitting plots reveal that the XGBT model exhibits outstanding predictive capability on both the training and testing sets, with nearly all predicted values closely aligned with the ideal diagonal line. RF and SVR also demonstrate strong performance, whereas the ANN and LR models show significant prediction deviations. In particular, LR substantially overestimates or underestimates the stability of several samples, making it the least effective model. This observation is further supported by the bar charts of error metrics, where the XGBT model consistently achieves the

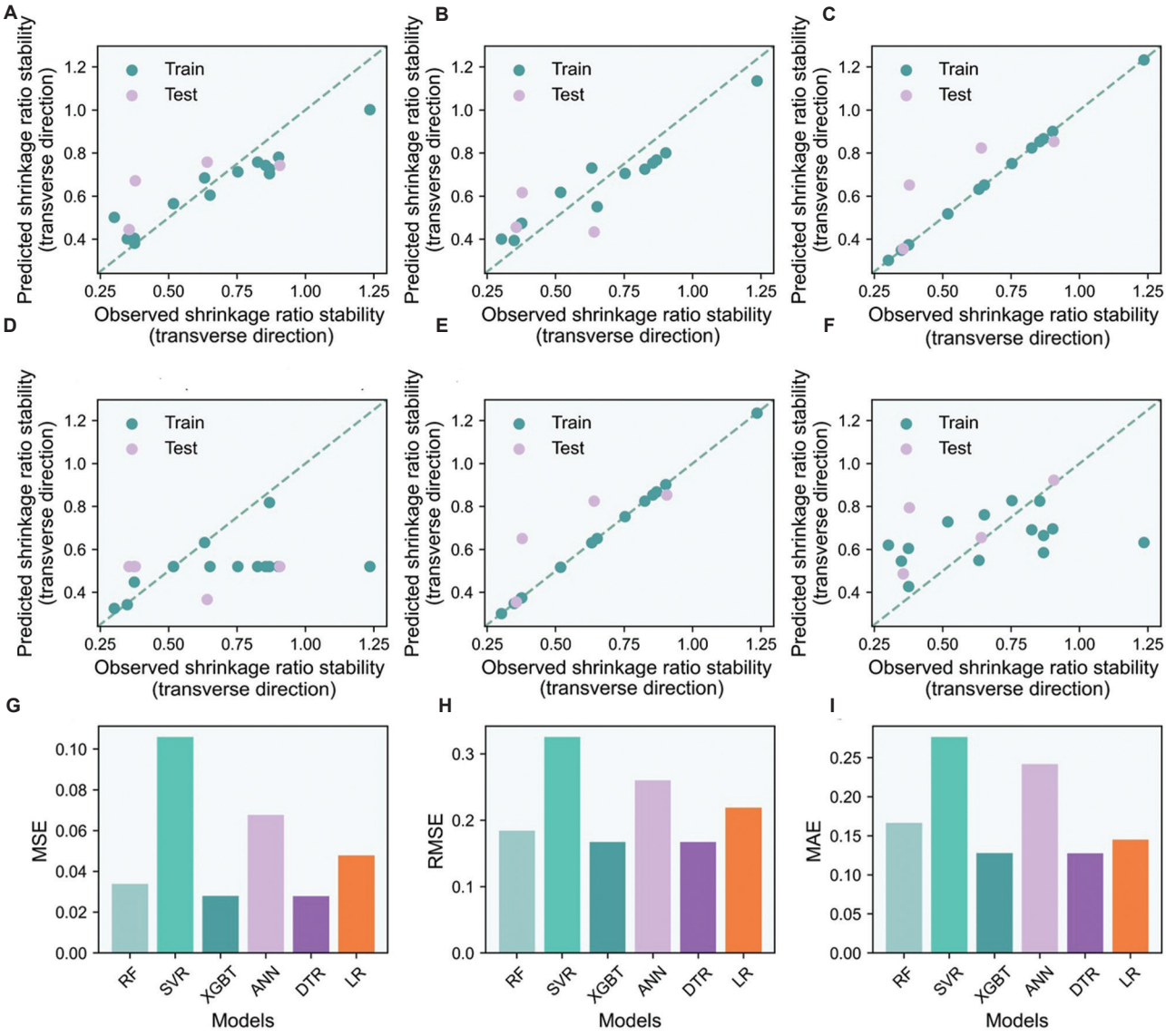

Figure 5. Performance of different machine learning models in predicting the stability of %TD on the test set. (A) RF. (B) SVR. (C) XGBT. (D) ANN. (E) DTR. (F) LR. (G) MSE of the models. (H) RMSE of the models. (I) MAE of the models.

Abbreviations: %TD: Shrinkage ratio (%) in transverse direction; ANN: Artificial neural networks; DTR: Decision tree regressor; LR: Linear regression; MAE: Mean absolute error; MSE: Mean squared error; RF: Random forest; RMSE: Root mean square error; SVR: Support vector regression; XGBT: Extreme gradient boosting trees.

lowest values in MSE and RMSE, confirming its superior accuracy and robustness in modeling TD stability. In contrast, the ANN and LR models yield significantly higher errors, indicating poor predictive reliability. Overall, the results indicate that XGBT is the most effective model for predicting %RD stability and %TD stability, outperforming other approaches in both accuracy and robustness.

3.3. Model interpretation by SHAPs

Figures 6 and 7 present the mean absolute SHAP values for the stability predictions of %RD and %TD, respectively, which quantify the relative importance of the four input features: Applied voltage, TPU concentration, collector speed, and distance between electrodes. These SHAP values represent the average magnitude of each feature's contribution to the model's output across all samples, thereby enabling a global interpretation of feature relevance. However, it is important to note that while SHAP values effectively capture feature importance, they do not indicate the directionality of influence; in other words, they do not reveal whether an increase in a given parameter enhances or diminishes stability. Applied voltage and TPU concentration consistently rank as the most influential factors in both RD and TD stability models, underscoring their critical role in governing shrinkage stability during electrospinning. Voltage controls the electrostatic field strength, directly influencing jet acceleration, elongation, and fiber morphology.[6,11,39-41] Even slight variations can induce significant changes in jet dynamics and deposition patterns, thereby altering internal stress distributions and post-activation stability. TPU concentration affects the solution's viscosity and molecular entanglement,[42,43] helping to stabilize jet morphology and reduce deformation. Speed and distance contribute less, suggesting a more indirect impact. Collector speed can affect fiber alignment,

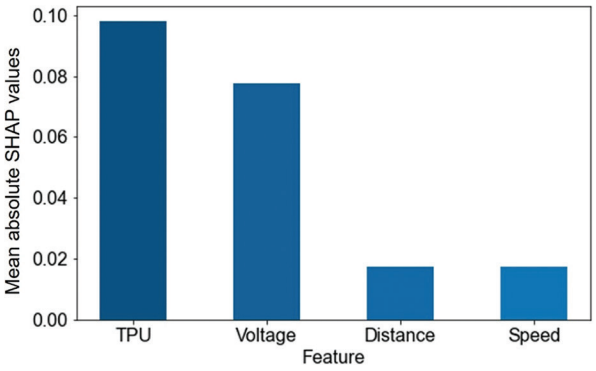

Figure 6. The mean absolute SHAP values of features for the percentage of rotational direction
Abbreviations: SHAP: Shapley additive explanations; TPU: Thermoplastic polyurethane.

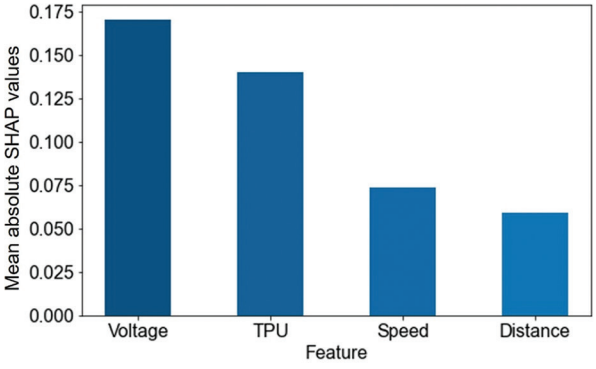

Figure 7. The mean absolute SHAP values of features for the percentage of the transverse direction
Abbreviations: SHAP: Shapley additive explanations; TPU: Thermoplastic polyurethane.

Table 2. Partial results of Pareto front screening obtained by the Monte Carlo method

TPU (%)	Distance (cm)	Speed (rpm)	Voltage (kV)	%RD	%TD	CIW
15	8	701	13	26.36	15.43	0.36
15	9	700	13	25.69	16.48	0.37
15	9	705	13	25.76	16.44	0.37
15	9	707	13	25.78	16.43	0.38
15	9	709	13	25.81	16.41	0.38
15	8	715	13	26.57	15.31	0.38
15	8	716	13	26.58	15.31	0.38
15	9	711	13	25.83	16.40	0.38
15	8	718	13	26.61	15.29	0.38
15	8	723	13	26.68	15.26	0.39
15	8	724	13	26.69	15.25	0.39
15	8	726	13	26.72	15.24	0.39
15	9	727	13	26.03	16.29	0.40
15	9	732	13	26.08	16.27	0.40
15	8	769	14	23.48	17.00	0.41
15	8	770	14	23.49	16.99	0.41
15	8	772	14	23.52	16.99	0.41
15	9	740	13	26.17	16.23	0.41
15	8	773	14	23.53	16.99	0.41
15	8	745	13	26.94	15.15	0.41
15	8	776	14	23.58	16.98	0.42
15	9	745	13	26.22	16.21	0.42
15	9	745	13	26.22	16.21	0.42
15	8	778	14	23.60	16.98	0.42
15	8	780	14	23.63	16.98	0.42

Abbreviations: %RD: Shrinkage ratio (%) in rotational direction; %TD: Shrinkage ratio (%) in transverse direction; CIW: Confidence interval width; TPU: Thermoplastic polyurethane.

potentially influencing %RD more than %TD. Distance influences jet flight time and solvent evaporation, but its effect appears less consistent. Although SHAP values cannot reveal directional effects, the results highlight voltage and polymer concentration as key parameters for controlling shape stability.

3.4. Monte Carlo simulation-based optimization

In electrospinning, required shrinkage ratios (%RD and %TD) vary across applications. To enable customized control of target shrinkage while maximizing process stability, we developed a process optimization framework that combines shrinkage prediction and stability prediction models. Using %RD = 25% and %TD = 15% with a ± 2% tolerance as a representative case to demonstrate the optimization process, 10,000 sets of process parameters were randomly generated via Monte Carlo sampling. These parameter sets were first evaluated by the shrinkage prediction model to identify those that met the target range. The qualified candidates were then assessed using the stability prediction model, which outputs the predicted CIW for both %RD and %TD. Since a smaller CIW indicates higher process stability, the parameter set with the minimum combined CIW was selected as the optimal condition. This approach enables simultaneous optimization of shrinkage accuracy and process robustness in electrospinning.

Table 2 presents a subset of process conditions generated via Monte Carlo simulation and screened using the shrinkage prediction model to meet the target values of %RD = 25% ± 2% and %TD = 15% ± 2%. Although all candidates fall within the target range, their predicted CIW vary from 0.36 to 0.42. The combination with the lowest CIW (TPU = 15%, distance = 8 cm, speed = 701 rpm, voltage = 13 kV) shows the highest predicted stability, indicating reduced sensitivity to process variability while maintaining the desired shrinkage levels.

Figure 8 shows the scatter plots of %RD and %TD for the Pareto-optimal sets across four key process variables, including TPU concentration (%), distance (cm), speed (rpm), and voltage (kV). As the TPU concentration was fixed at 15%, no variation is observed in Figure 8A. Figure 8B shows minor fluctuations in %RD and %TD at collector distances of 8 cm and 9 cm. In Figure 8C, %RD decreased notably at speeds above 800 rpm, whereas %TD

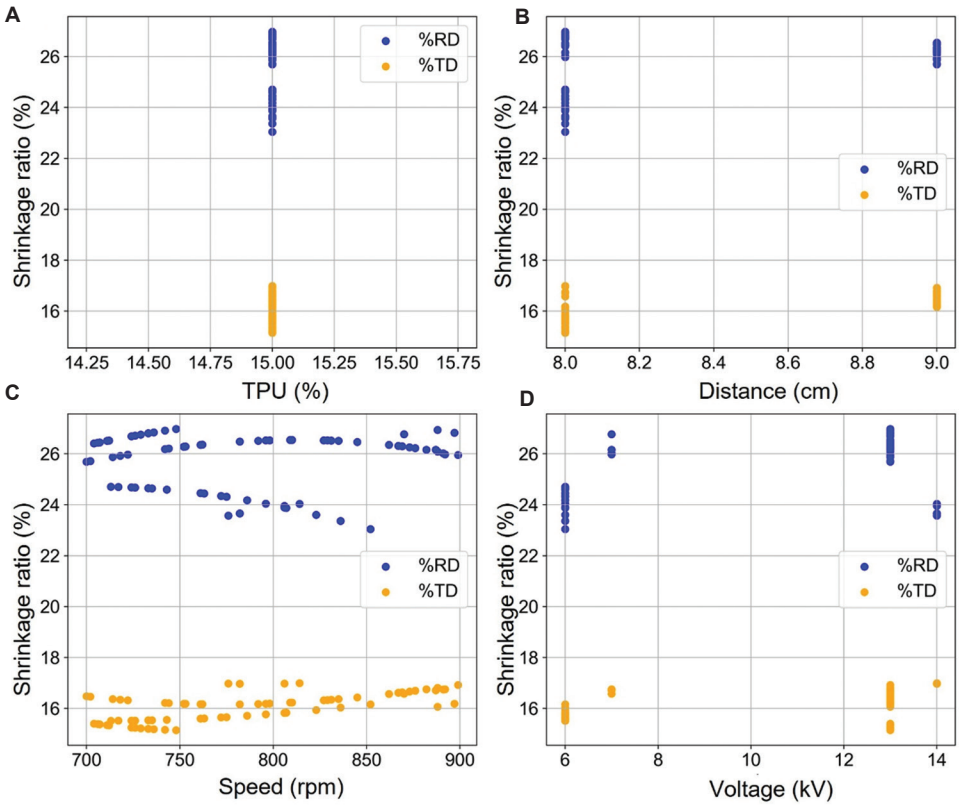

Figure 8. Scatter plots of each feature versus %RD and %TD in the results of the Pareto front. (A) TPU concentration (%). (B) Distance (cm). (C) Speed (rpm). (D) Voltage (kV).
Abbreviations: %RD: Shrinkage ratio (%) in rotational direction; %TD: Shrinkage ratio (%) in transverse direction; TPU: Thermoplastic polyurethane.

exhibited a slight increase. In Figure 8D, both %RD and %TD elevated with increasing voltage, indicating voltage as a key parameter in shrinkage control. These results demonstrate that meeting shrinkage targets alone is insufficient for ensuring process reliability. Incorporating CIW as a stability metric allows selection of process conditions that are both accurate and robust, providing a practical basis for optimizing electrospinning parameters in scalable production.

The machine learning models in this study were developed and validated using experimental data from controlled electrospinning trials of TPU membranes, with repeated measurements used to capture both mean shrinkage and variability via the CIW metric. Monte Carlo optimization was conducted on these validated models within practical parameter ranges, ensuring physically relevant predictions. The modeling framework is material-agnostic and, in principle, applicable to other polymers; extending it requires retraining with high-quality data specific to the target material to capture its unique processing-structure-property relationships. Direct experimental validation of our multi-objective optimization framework was not performed due to the high cost and time required. Future work will address this to further enhance the model's robustness and generalizability.

4. Conclusion

This paper presents a data-driven framework that combines machine learning with Monte Carlo simulation to achieve accurate and stable control of biaxial shrinkage in electrospun membranes, even under limited data conditions.

By modeling shrinkage ratios in both RD and TD along with their stability, the framework enables multi-objective optimization of process parameters. Among the evaluated models, SVR demonstrated the highest accuracy in predicting shrinkage behavior, achieving an RMSE of 1.04% for RD and 2.00% for TD. XGBT was most effective in forecasting shrinkage stability, with RMSE of 0.16 for RD and 0.17 for TD. SHAP analysis identified applied voltage and TPU concentration as the most influential factors governing shrinkage stability, whereas collector speed and distance between electrodes had relatively minor effects.

Using the Monte Carlo-based parameter screening, the framework successfully identified sets of process parameters that met predefined shrinkage targets while minimizing variability.

In conclusion, this methodology offers a robust and generalizable strategy for high-variability, small-sample manufacturing scenarios, with significant potential for broader applications in smart material design and precision fabrication.

Acknowledgments

None.

Funding

This work was funded by the National Natural Science Foundation of China (grant no.: 52031005, 52571227), Natural Science Foundation of Shanghai (grant no.: 24ZR1438200), Shanghai Academy of Spaceflight Technology Joint Research Fund (grant no.: USCAST2023-19), Equipment Development Department Huiyan Action (grant no.: 5D3D1365), and China Scholarship Council (grant no.:202406230025).

Conflict of interest

The authors declare they have no competing interests.

Author contributions

Conceptualization: Wei Min Huang, Shiyu He
Formal analysis: Shiyu He, Li Cong Huang
Investigation: Shiyu He, Wei Min Huang, Fei Xiao
Methodology: Shiyu He, Chentong Gao, Runzhi Lu
Writing–original draft: Shiyu He, Wei Min Huang
Writing–review & editing: Shiyu He, Wei Min Huang, Fei Xiao

Ethics approval and consent to participate

Not applicable.

Consent for publication

Not applicable.

Availability of data

Data are available from the corresponding author upon reasonable request.

References

1. Cheng F, Song D, Li H, Ravi SK, Tan SC. Recent progress in biomedical scaffold fabricated via electrospinning: Design, fabrication and tissue engineering application. *Adv Funct Mater*. 2025;35(1):2406950.

   doi: 10.1002/adfm.202406950

2. Cho Y, Beak JW, Sagong M, Ahn S, Nam JS, Kim ID. Electrospinning and nanofiber technology: Fundamentals, innovations, and applications. *Adv Mater*. 2025;37:2500162.

   doi: 10.1002/adma.202570190

3. Wang C, Su Y, Xie J. Advances in electrospun nanofibers: Versatile materials and diverse biomedical applications. *Acc*

Mater Res. 2024;5(8):987-999.

doi: 10.1021/accountsmr.4c00145

4. Yadav S, Sharma A, Kurmi BD, *et al*. Nanofiber drug delivery systems: Recent advances in nanofabrication and their role in targeted therapy in cancer, neurodegenerative, and cardiovascular diseases. *Polym Adv Technol*. 2025;36(5):e70198.

   doi: 10.1002/pat.70198

5. Wang Z, Gao C, Yang R, Xiong F. The interface effect of electrospun fiber promotes wound healing. *Macromol Rapid Commun*. 2025:2500038.

   doi: 10.1002/marc.202500038

6. Wang J, You C, Xu Y, Xie T, Wang Y. Research advances in electrospun nanofiber membranes for non-invasive medical applications. *Micromachines*. 2024;15(10):1226.

   doi: 10.3390/mi15101226

7. Wu H, Zheng Y, Zeng Y. Fabrication of helical nanofibers via co-electrospinning. *Ind Eng Chem Res*. 2015;54(3):987-993.

   doi: 10.1021/ie504305s

8. Zhao Y, Miao X, Lin J, *et al*. Coiled plant tendril bioinspired fabrication of helical porous microfibers for crude oil cleanup. *Glob Challenges*. 2017;1(3):1600021.

   doi: 10.1002/gch2.201600021

9. Wang M, Li W, Tang G, Garciamendez Mijares CE, Zhang YS. Engineering (bio) materials through shrinkage and expansion. *Adv Healthc Mater*. 2021;10(14):2100380.

   doi: 10.1002/adhm.202100380

10. Mandal A, Chatterjee K. 4D printing for biomedical applications. *J Mater Chem B*. 2024;12(12):2985-3005.

    doi: 10.1039/D4TB00006D

11. Fang F, Wang H, Wang H, *et al*. Stimulus-responsive shrinkage in electrospun membranes: Fundamentals and control. *Micromachines*. 2021;12(8):920.

    doi: 10.3390/mi12080920

12. Zaarour B, Liu W, Omran W, *et al*. A mini-review on wrinkled nanofibers: Preparation principles via electrospinning and potential applications. *J Ind Text*. 2024;54:15280837241255396.

    doi: 10.1177/15280837241255396

13. Wang CC, Zhao Y, Purnawali H, Huang WM, Sun L. Chemically induced morphing in polyurethane shape memory polymer micro fibers/springs. *React Funct Polym*. 2012;72:757-764.

    doi: 10.1016/j.reactfunctpolym.2012.07.013

14. Aadithiya D, Fang FY, Wang H, Huang WM. Stimulus-induced shrinkage in electrospun polymeric fibres: An investigation on thickness of prestretched shell and prestrain via finite element analysis. *Fibers Polym*. 2023;24(2):525-536.

    doi: 10.1007/s12221-023-00133-8

15. Ahmadi Bonakdar M, Rodrigue D. Electrospinning: Processes, structures, and materials. *Macromol*. 2024;4(1):58-103.

    doi: 10.3390/macromol4010004

16. El Ferik S, Adeniran AA. Modeling and identification of nonlinear systems: A review of the multimodel approach-Part 2. *IEEE Trans Syst Man Cybern Syst*. 2016;47(7):1160-1168.

    doi: 10.1109/TSMC.2016.2560129

17. Subeshan B, Atayo A, Asmatulu E. Machine learning applications for electrospun nanofibers: A review. *J Mater Sci*. 2024;59(31):14095-14140.

    doi: 10.1007/s10853-024-09994-7

18. Shastry T, Basdogan Y, Wang ZG, Kunmar SK, Carbone MR. Machine learning-based discovery of molecular descriptors that control polymer gas permeation. *J Membr Sci*. 2024;697:122563.

    doi: 10.1016/j.memsci.2024.122563

19. Ignacz G, Beke AK, Toth V, Szekely G. A hybrid modelling approach to compare chemical separation technologies in terms of energy consumption and carbon dioxide emissions. *Nat Energy*. 2025;10(3):308-317.

    doi: 10.1038/s41560-024-01668-7

20. Lee S, Shirts MR, Straub AP. Molecular fingerprint-aided prediction of organic solute rejection in reverse osmosis and nanofiltration. *J Membr Sci*. 2024;705:122927.

    doi: 10.1016/j.memsci.2024.122927

21. He S, Wang Y, Zhang Z, *et al*. Interpretable machine learning workflow for evaluation of the transformation temperatures of TiZrHfNiCoCu high entropy shape memory alloys. *Mater Des*. 2023;225:111513.

    doi: 10.1016/j.matdes.2022.111513

22. He SY, Xiao F, Hou RH, *et al*. Accelerated learning and co-optimization of elastocaloric effect and stress hysteresis of elastocaloric alloys. *Rare Met*. 2024;43(12):6606-6624.

    doi: 10.1007/s12598-024-02827-1

23. Rigatti SJ. Random forest. *J Insur Med*. 2017;47(1):31-39.

    doi: 10.17849/insm-47-01-31-39.1

24. Osman AIA, Ahmed AN, Chow MF, Huang YF, EI-Shafle A. Extreme gradient boosting (Xgboost) model to predict the groundwater levels in Selangor Malaysia. *Ain Shams Eng J*. 2021;12(2):1545-1556.

    doi: 10.1016/j.asej.2020.11.011

25. Zou J, Han Y, So SS. Overview of artificial neural networks. In: *Artificial Neural Networks: Methods and Applications*.

Springer; 2009.

doi: 10.1007/978-1-60327-101-1_2

26. Su X, Yan X, Tsai CL. Linear regression. *Wiley Interdiscip Rev Comput Stat*. 2012;4(3):275-294.

doi: 10.1002/wics.1198

27. Mosca E, Szigeti F, Tragianni S, Gallagher D, Groh G. SHAP-based explanation methods: A review for NLP interpretability. In: *Proceedings of the 29th International Conference on Computational Linguistics*; 2022.

doi: 2022.coling-1.406

28. Antwarg L, Miller R M, Shapira B, Rokach L. Explaining anomalies detected by autoencoders using Shapley Additive Explanations. *Expert Syst Appl*. 2021;186:115736.

doi: 10.1016/j.eswa.2021.115736

29. Van den Broeck G, Lykov A, Schleich M, Suciu D. On the tractability of SHAP explanations. *J Artif Intell Res*. 2022;74:851-886.

doi: 10.1613/jair.1.13283

30. Li Z. Extracting spatial effects from machine learning model using local interpretation method: An example of SHAP and XGBoost. *Comput Environ Urban Syst*. 2022;96:101845.

doi: 10.1016/j.compenvurbsys.2022.101845

31. Zhang J, Ma X, Zhang J, *et al*. Insights into geospatial heterogeneity of landslide susceptibility based on the SHAP XGBoost model. *J Environ Manag*. 2023;332:117357.

doi: 10.1016/j.jenvman.2023.117357

32. Wang H, Liang Q, Hancock JT, Khoshgoftaar TM. Feature selection strategies: A comparative analysis of SHAP value and importance based methods. *J Big Data*. 2024;11(1):44.

doi: 10.1186/s40537-024-00905-w

33. Harrison RL. Introduction to monte carlo simulation. *AIP Conf Proc*. 2010;1204:17.

doi: 10.1063/1.3295638

34. Metropolis N, Ulam S. The monte carlo method. *J Am Stat Assoc*. 1949;44(247):335-341.

doi: 10.2307/2280232

35. Raychaudhuri S. Introduction to monte carlo simulation. In: *Proceedings of the 2008 Winter Simulation Conference*; 2008.

doi: 10.1109/WSC.2008.4736059

36. Kroese DP, Rubinstein RY. Monte carlo methods. *Wiley Interdiscip Rev Comput Stat*. 2012;4(1):48-58.

doi: 10.3390/nano15020117

37. Kroese DP, Brereton T, Taimre T, *et al*. Why the Monte Carlo method is so important today. *Wiley Interdiscip Rev Comput Stat*. 2014;6(6):386-392.

doi: 10.1002/wics.1314

38. Gao H, He W, Zhao YB, Opris DM, Xu G, Wang J. Electret mechanisms and kinetics of electrospun nanofiber membranes and lifetime in filtration applications in comparison with corona charged membranes. *J Membr Sci*. 2020;600:117879.

doi: 10.1016/j.memsci.2020.117879

39. Tong HW, Wang M. Electrospinning of fibrous polymer scaffolds using positive voltage or negative voltage: A comparative study. *Biomed Mater*. 2010;5(5):054110.

doi: 10.1088/1748-6041/5/5/054110

40. Liao Y, Wang R, Tian M, Qiu C, Fane AG. Fabrication of polyvinylidene fluoride (PVDF) nanofiber membranes by electro spinning for direct contact membrane distillation. *J Membr Sci*. 2013;425:30-39.

doi: 10.1016/j.memsci.2012.09.023

41. Mi HY, Jing X, Jacques BR, Turng LS, Peng XF. Characterization and properties of electrospun thermoplastic polyurethane blend fibers: Effect of solution rheological properties on fiber formation. *J Mater Res*. 2013;28(17):2339-2350.

doi: 10.1016/j.memsci.2012.09.023

42. Lem KW, Haw JR, Curran S, *et al*. Effect of hard segment molecular weight on dilute solution properties of ether based thermoplastic polyurethanes. *Spectroscopy*. 2013;1:11-18.

doi: 10.13189/nn.2013.01030

43. Awad M, Khanna R. Support vector regression. In: *Efficient Learning Machines: Theories, Concepts, and Applications for Engineers and System Designers*. Springer; 2015.

doi: 10.1007/978-1-4302-5990-9